

Electronic supplementary information

Giant mechanical tunability by coordination bond strategy in a 3D hybrid cyanide double perovskite ferroelastic with reconstructive phase transition

Hui-Peng Lv,[‡] Sheng-Qian Hu,[‡] Yong-Ju Bai, Jun-Si Zhou, Luan-Ying Ji, Zhong-Xia Wang, Yong Ai, Yan Qin,* and Xiao-Gang Chen*

Ordered Matter Science Research Center, Nanchang University, Nanchang 330031, People's Republic of China.

E-mail: qinyan@ncu.edu.cn, chenxg@ncu.edu.cn.

Experimental Section

Synthesis of EAOH-1

All chemicals were commercially available and were used without further purification. Ethanolamine hydrochloride (4.877 g, 50 mmol) was added to 25 ml aqueous solution of $K_3Fe(CN)_6$ (3.29 g, 10 mmol). Place the solution in a low-temperature (291~303 K) light-protected drying environment. Reddish brown block crystals of EAOH-1 were obtained after two weeks.

Synthesis of EAOH-2

All chemicals were commercially available and used without further purification. Ethanolamine hydrochloride (4.877 g, 50 mmol) was added to a 25 ml aqueous solution of $K_3Fe(CN)_6$ (3.29 g, 10 mmol). The solution was placed in a 318 K light-protected drying oven. Reddish brown block crystals of EAOH-2 were obtained after a week.

Synthesis of EA

All chemicals were commercially available and were used without further purification. Ethylamine hydrochloride (6.849 g, 84 mmol) was added to 20 ml aqueous solution of $K_3Fe(CN)_6$ (3.951 g, 12 mmol). Place the solution together with solid sodium hydroxide in a light-protected drying oven. Brownish-black block crystals of EA were obtained at room temperature after eight days.

Differential Scanning Calorimetry (DSC)

Thermal analysis measurements of EAOH-1 were performed on the Perkin-Elmer Diamond DSC instrument. The powder sample was placed in aluminum crucibles and measured under a nitrogen atmosphere at heating and cooling rates of $10\text{ K}\cdot\text{min}^{-1}$.

Dielectric Measurements

The powder-pressed pellets of EAOH-1 coated with silver conducting glue on both sides were used in dielectric measurements. The temperature-dependent dielectric constant was measured on a TH2828A impedance analyzer at 1 MHz with an applied voltage of 1 V.

Single-crystal X-ray Crystallography

Variable-temperature single-crystal X-ray diffraction data were gathered using a Rigaku XtaLAB Synergy-R/DW diffractometer with Cu-K α radiation ($\lambda = 1.54178\text{ \AA}$) (for data at 300 K and 368 K) and Mo-K α radiation ($\lambda = 0.71073\text{ \AA}$) (for data at 388 K as well as 300 K and 100 K after heating to 368 K). A single crystal with approximate dimensions of $0.2 \times 0.1 \times 0.1\text{ mm}^3$ was selected for SCXRD measurements. The crystal was mounted on a homemade glass fiber using a high-temperature-resistant glue. Data collection was conducted at a controlled temperature with a heating/cooling rate of 20 K/min. Data collection and structural refinement were performed using the Rigaku Crystal Clear and SHELXTL software package. The crystal data and structure refinement of EAOH-1 are summarized in Table S3-S6. The X-ray crystallographic structures have been deposited at the Cambridge Crystallographic Data Centre (deposition numbers CCDC: 2417523-2417525 and 2434342-2434343) and can be obtained free of charge from the CCDC via www.ccdc.cam.ac.uk/getstructures.

Powder X-ray Diffraction (PXRD)

PXRD data were measured on a Rigaku D/MAX 2000 PC X-ray diffractometer with Cu-K α radiation. PXRD measurements were performed using a flat plate sample holder. The heating/cooling rate was set to 20 K/min. Diffraction patterns were collected in the 2θ range of 5–50° with a step size of 0.02°. Simulation of the PXRD spectrum was carried out by the single-crystal data and diffraction-crystal module of the Mercury program.

Optical microscopy measurements

Ferroelastic domain observations were carried out using an OLYMPUS BX53-P polarizing microscope. The temperature was controlled by a Linkam LTS420 cooling/heating stage with a rate of 10 K/min.

Raman spectroscopy

Raman spectra were measured by a Raman spectrometer (Horiba, LabRAM HR Evolution) under a 633 nm excitation with the reflection method. The spectrum was dispersed by a 600 groove per millimeter diffraction grating and accumulated 2 times with exposure for 2 s. The temperature-dependent Raman spectra were detected by loading the sample in a temperature controller (Linkam, LNP96-S).

Infrared spectroscopy

Infrared (IR) spectra was measured on a FT-IR Spectrometers (INVENIO R, Bruker) using KBr pellet method. The sample (5 mg) was mixed with KBr (95 mg) and well grounded into powder, and then the mixture was pressed into a thin and transparent sheet for measurement.

Nanoindentation Characterization

The nanoindentation test was carried out on the Hysitron TI Premier nanoindentation instrument, and the Berk probe applied a load to form a pit. The crystal with a smooth surface was adhered to the steel SPM wafer by UV glue. Due to the static magnetic force, the SPM wafer was fixed on the instrument table. Nanoindentation measurements were performed using a three-sided pyramidal Berkovich tip in the continuous stiffness measurement (CSM) mode. Variable temperature nanoindentation measurements were performed for EAOH-1, while others were tested at room temperature. The initial loading amplitude was set to 5 %, with loading, holding, and unloading times of 32 s, 2 s, and 5 s, respectively. In order to reduce accidental errors, indentation curves were collected from different positions. Based on the Oliver-Pharr method, the elastic modulus and hardness values were obtained by fitting the indentation curve.

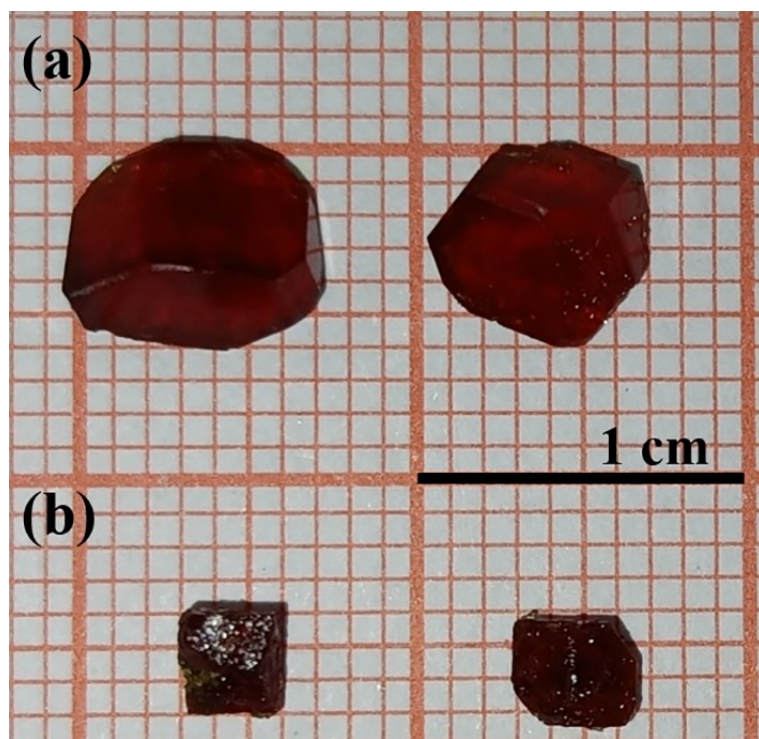


Fig. S1 Crystal morphology of compounds EAOH-1 (a) and EAOH-2 (b).

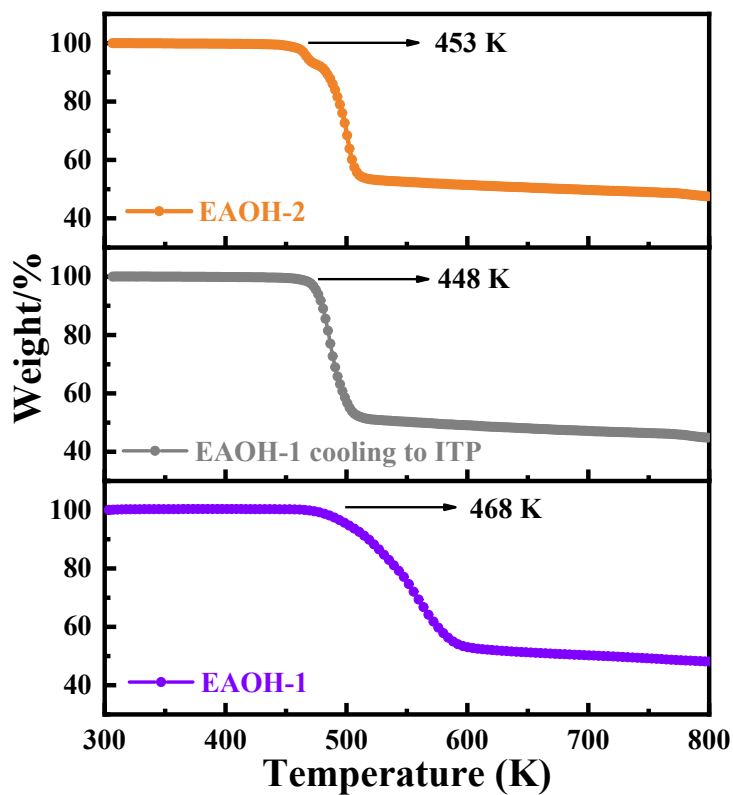


Fig. S2 TGA curves of compound EA, EAOH-1, and EAOH-2.

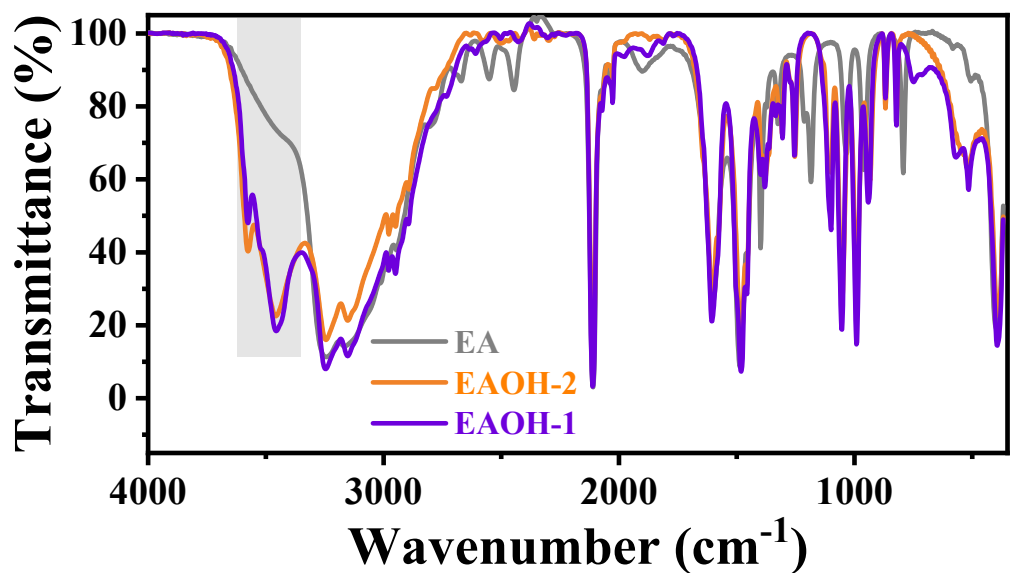


Fig. S3 IR spectra of EA, EAOH-1, and EAOH-2 at room temperature.

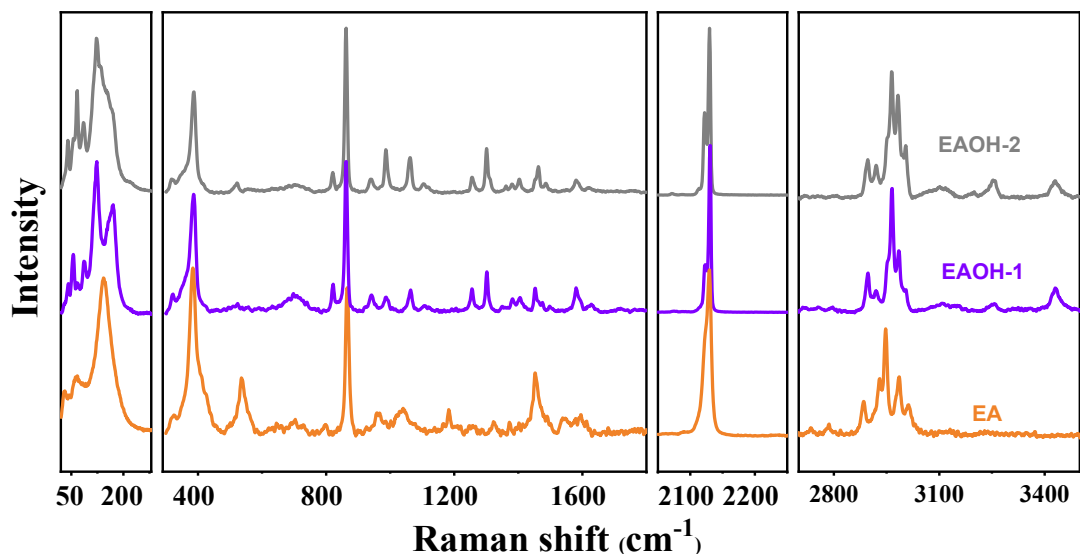


Fig. S4 Raman spectra of EA, EAOH-1, and EAOH-2 at room temperature.

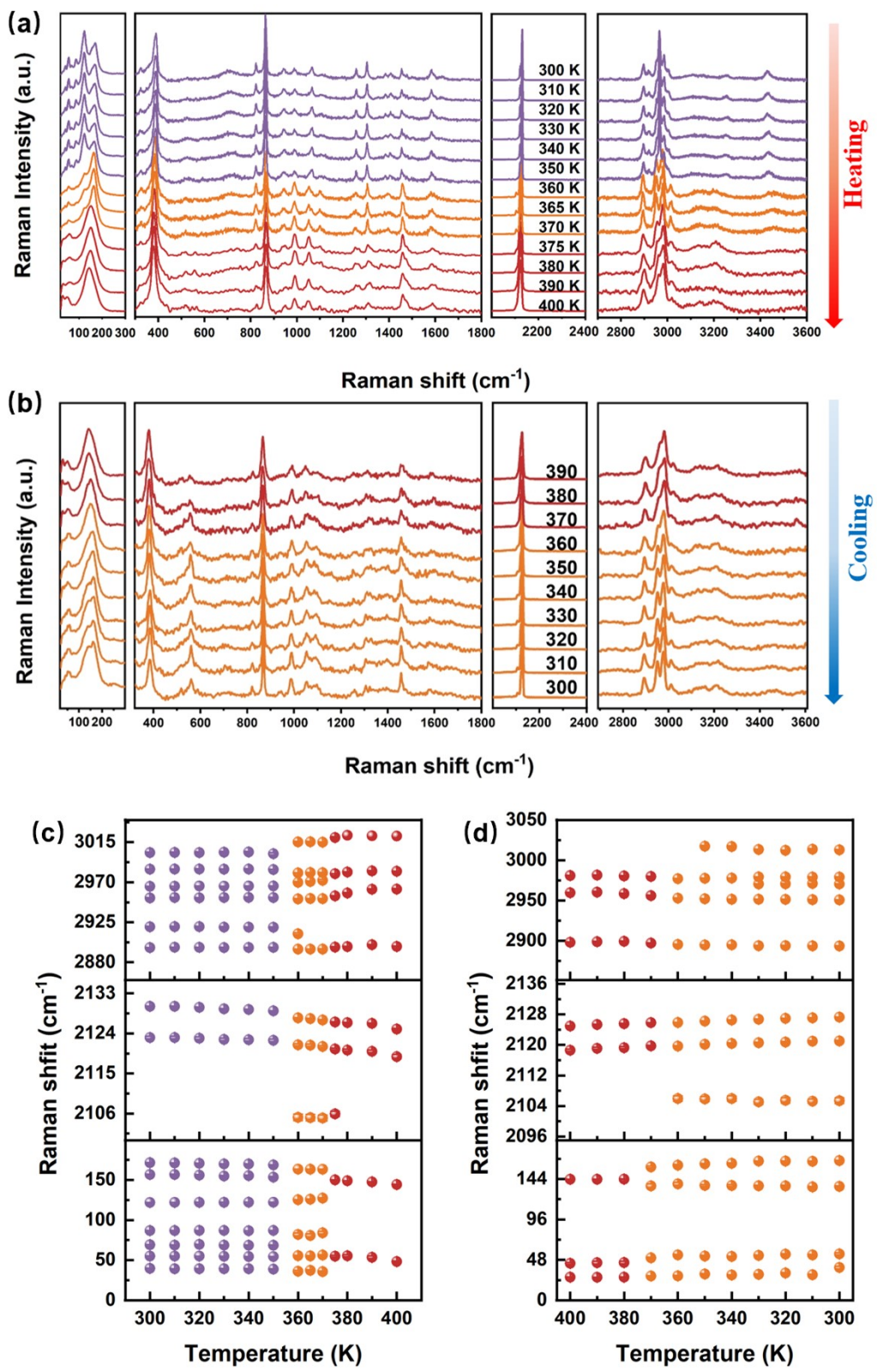


Fig. S5 (a-b) Temperature-dependent Raman spectra of EAOH-1 in the heating (a) and cooling run (b), respectively. Temperature dependence of Raman shifts in the heating (c) and cooling (d) run, respectively.

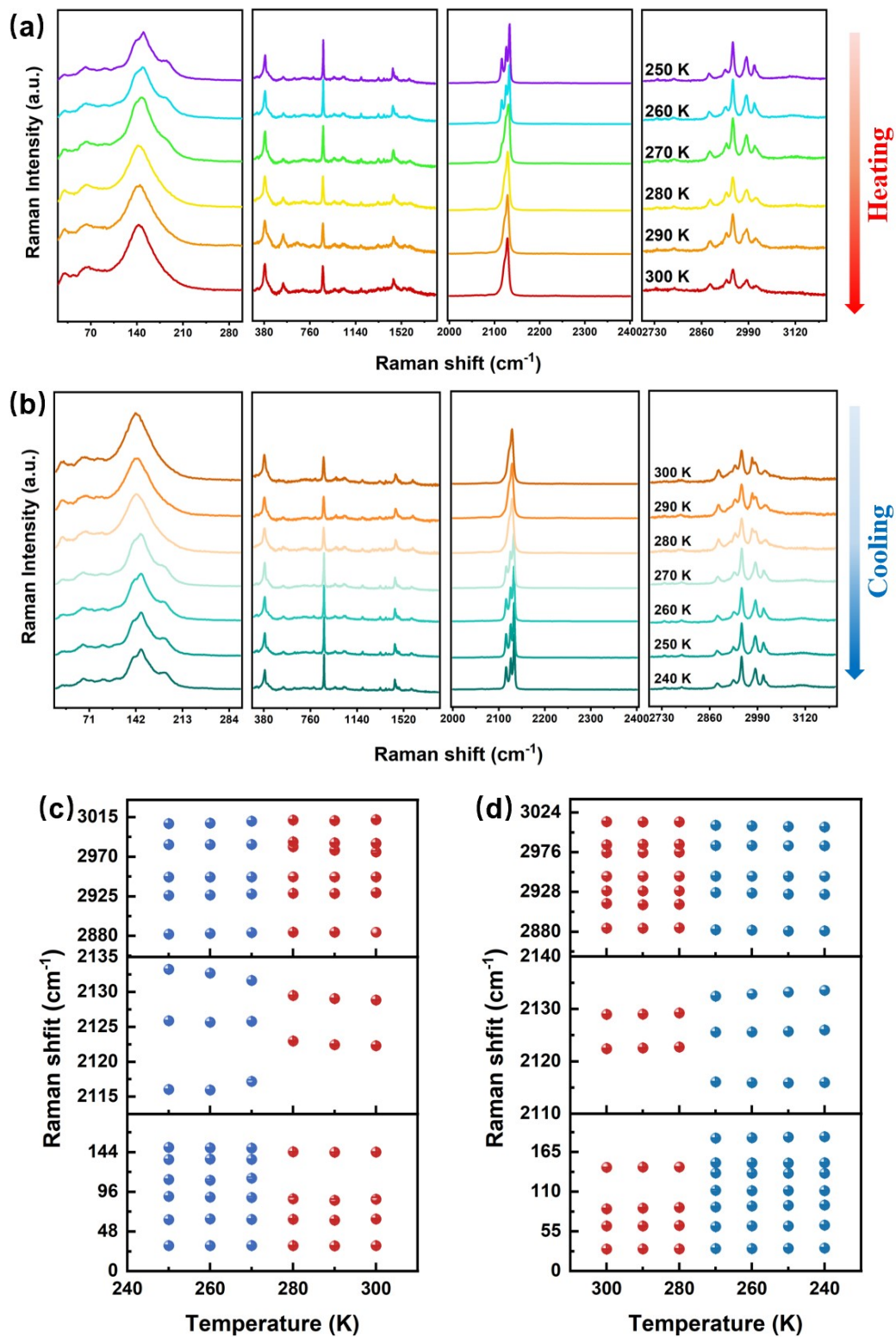


Fig. S6 (a-b) Temperature-dependent Raman spectra of EA in the heating (a) and cooling run (b), respectively. Temperature dependence of Raman shifts in the heating (c) and cooling (d) run, respectively.

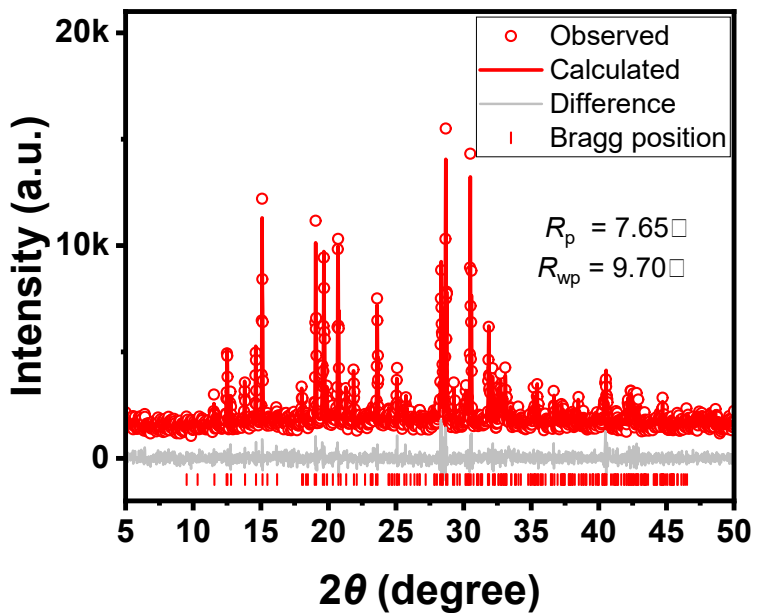


Fig. S7 Rietveld refinement result of PXRD pattern of EAOH-1 at 300 K.

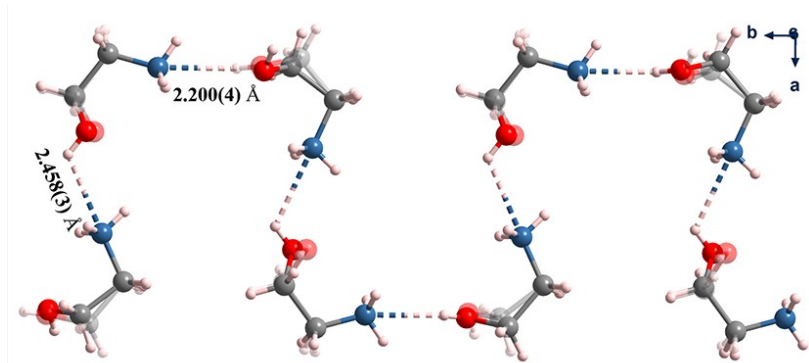


Fig. S8 One-dimensional hydrogen bonds between the adjacent organic cations of EAOH-1 at 368 K along the crystallography b -axis. The distance unit is Å.

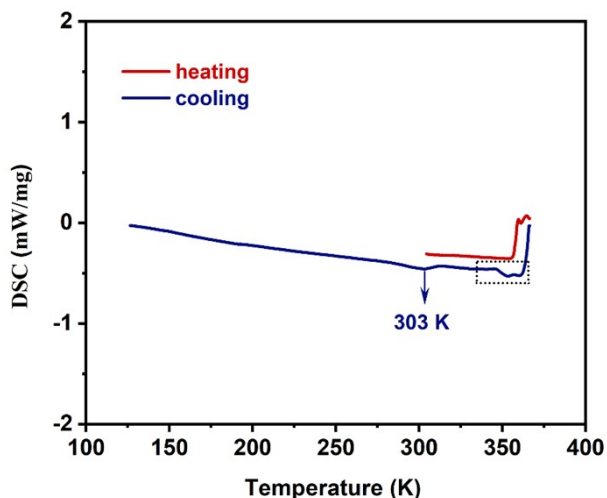


Fig. S9 DSC curve of EAOH-1 heated to 368 K and then cooled to 100 K. The peak within the black dashed box during the cooling process is caused by instrument calibration.

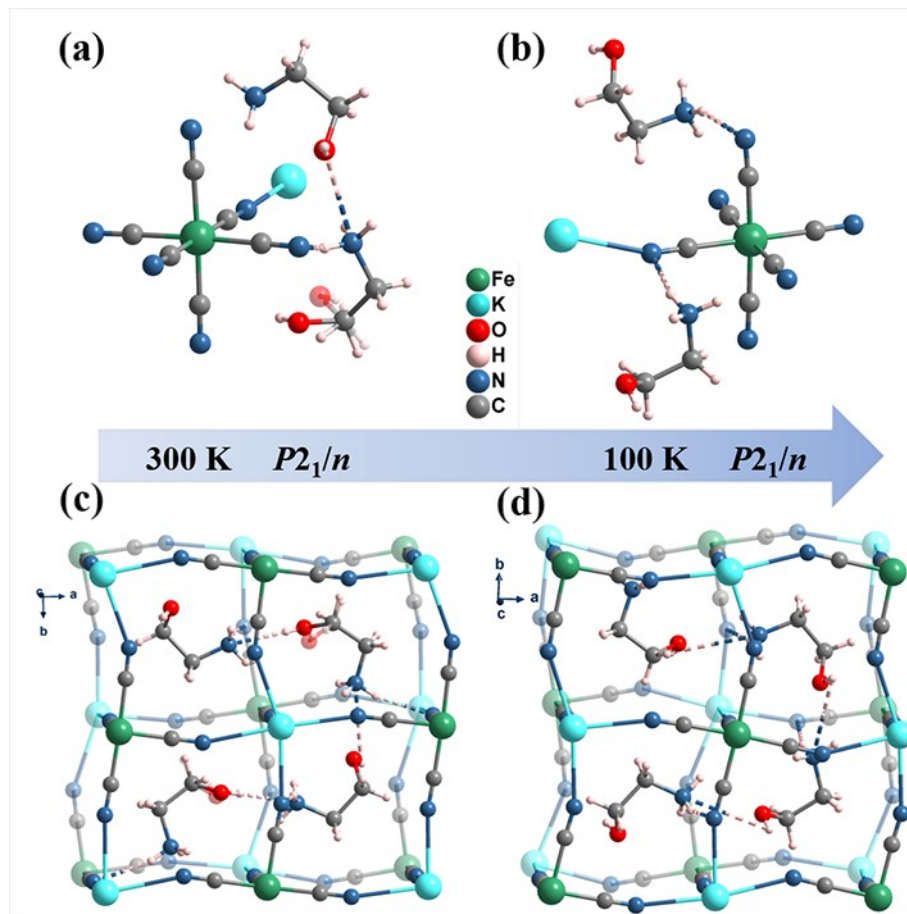


Fig. S10 Structural of the ITP of EAOH-1 at 300 K and 100 K. (a) The asymmetric unit of EAOH-1 in ITP at 300 K. (b) The asymmetric unit of EAOH-1 in ITP at 100 K. (c) Perspective view of packing structure of EAOH-1 in ITP at 300 K. (d) Perspective view of packing structure of EAOH-1 in ITP at 100 K.

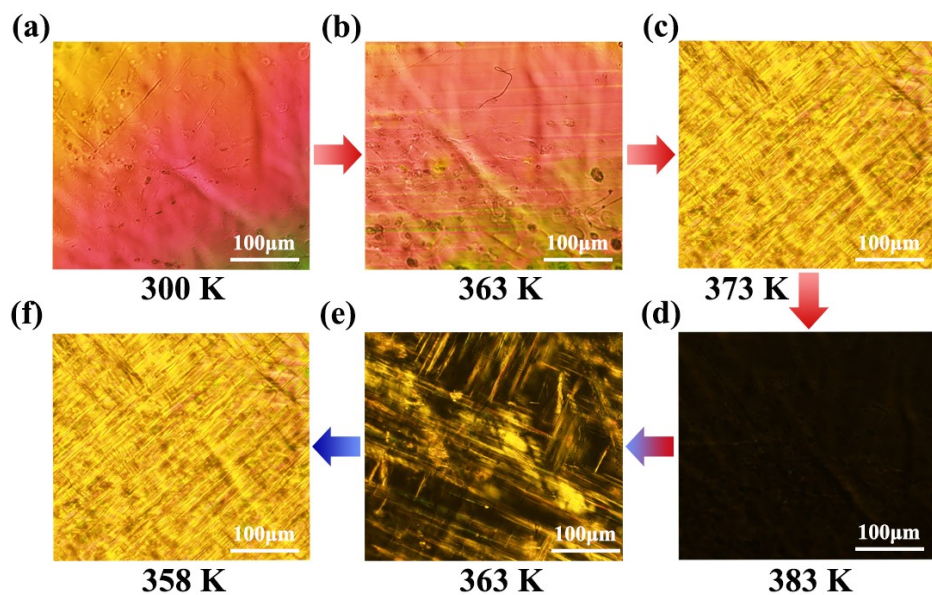


Fig. S11 Evolution of ferroelastic domains during the heating ((a)-(d)) and cooling process ((e) and (f)) for EAOH-1.

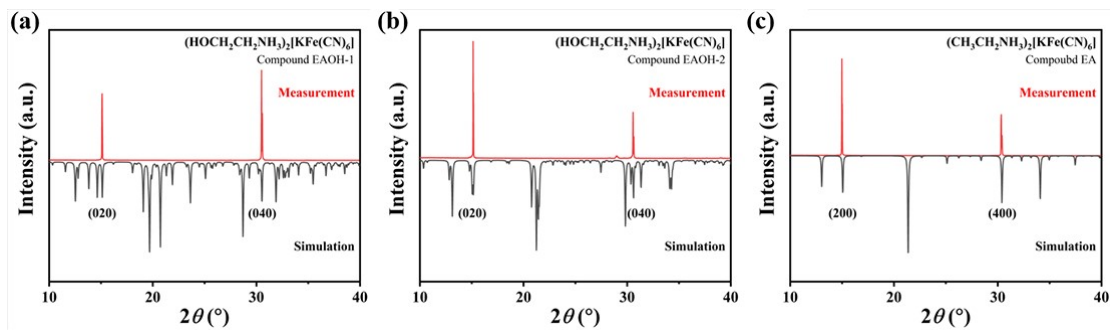


Fig. S12 Measured X-ray diffraction patterns of crystal plane in nanoindentation measurement and simulated patterns of compounds EAOH-1 (a), EAOH-2 (b), and EA (c).

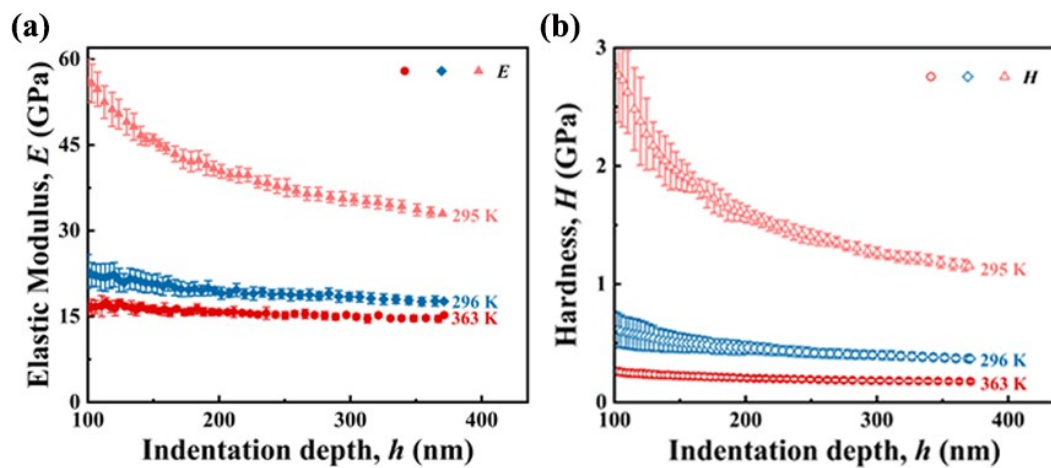


Fig. S13 (a) hardness as a function of indentation depth at different temperatures for EAOH-1. (b) The histogram of the elastic moduli and hardness of EAOH-1 measured at different temperatures.

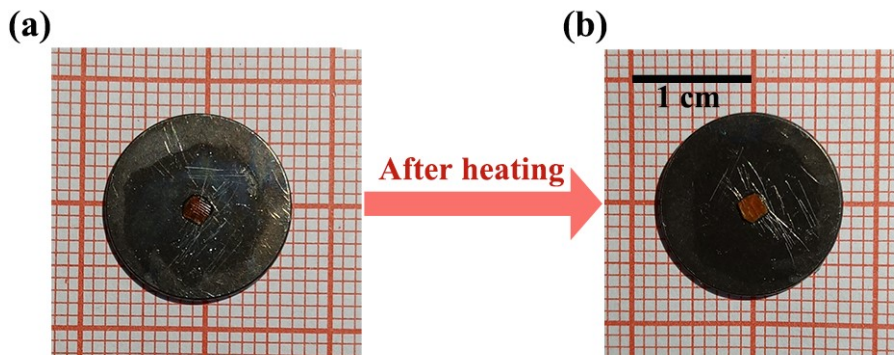


Fig. S14 Crystal morphology of compounds EAOH-1 before heating (a) and after a heating-cooling cycle (b) in the nanoindentation test.

Table S1. Raman wavenumbers (in cm^{-1}) of the LTP (300 K), ITP (370 K), HTP (390 K) of EAOH-1 together with the proposed assignment.

300 K (LTP)	370 K (ITP)	390 K (HTP)	assignment
3431	3459		$\nu(\text{OH})$
3256	3200	3205	$\nu_{\text{as}}(\text{NH}_3)$
3006	3013	3022	$\nu_{\text{as}}(\text{CH}_2)$
2985	2981	2982	$\nu_{\text{as}}(\text{CH}_2)$
2965	2950		$\nu_s(\text{CH}_2)$
2897	2895	2898	$\nu_s(\text{CH}_2)$
2130	2127	2126	$\nu(\text{CN})$
1583	1584	1589	$\delta_{\text{as}}(\text{NH}_3)$
1454	1458	1459	$\delta(\text{CH}_2)$
1407			$\delta_s(\text{NH}_3)$
1384	1386		$\omega(\text{CH}_2)$
1304	1306	1316	$\omega(\text{CH}_2)$
1257	1257	1257	$\tau(\text{CH}_2)$
1066	1050	1050	$\nu_{\text{as}}(\text{CCN})$
990	990	994	$\nu_s(\text{CCN})$
943	942		$\rho(\text{NH}_3)+\rho(\text{CH}_2)$
864	867	866	$\nu(\text{CC})$
823	822	824	$\tau(\text{HCCO})$
323	323	322	$\delta(\text{CCN})$
169+122	164+120	149	Lattice vibration modes
87			Lattice vibration modes
68			Lattice vibration modes
54	55	58	Lattice vibration modes
40	38	30	Lattice vibration modes

Table S2. Raman wavenumbers (in cm^{-1}) of the HTP (300 K) and LTP (240 K) of EA together with the proposed assignment.

300 K (HTP)	240 K (LTP)	assignment
3232	3238	$\nu_{\text{as}}(\text{NH}_3)$
3010	3005+3013	$\nu_{\text{as}}(\text{CH}_2)$
2975+2983	2984	$\nu_{\text{as}}(\text{CH}_2)$
2929+2946	2924+2946	$\nu_s(\text{CH}_2)$
2883	2881	$\nu_s(\text{CH}_2)$
2122+2128	2115+2126+2133	$\nu(\text{CN})$
1594	1584	$\delta_{\text{as}}(\text{NH}_3)$
1454	1448+1470+1484	$\delta(\text{CH}_2)$
1400	1401	$\delta_s(\text{NH}_3)$
1374	1375	$\omega(\text{CH}_2)$
1324	1329	$\omega(\text{CH}_2)$
1184	1187	$\rho(\text{CH}_2)$
1040	1038	$\nu_{\text{as}}(\text{CCN})$
970	963	$\rho(\text{NH}_3)+\rho(\text{CH}_2)$
867	871	$\nu(\text{CC})$
801	787	$\tau(\text{HOCC})$
	631	$\delta(\text{CCO})$
	540	$\delta(\text{CCO})$
385	389+325+311	$\delta(\text{CCN})$
141+127	184+149+138	Lattice vibration modes
	111	Lattice vibration modes
83	92	Lattice vibration modes
63	62	Lattice vibration modes
30	32	Lattice vibration modes

Table S3. Crystal data and structure refinement of EAOH-1 at 300 K, 368 K, and 388 K.

Compound	EAOH-1		
Temperature	300 K	368 K	388 K
Phase	LTP	ITP	HTP
Formula	$C_{10}H_{16}FeKN_8O_2$	$C_{10}H_{16}FeKN_8O_2$	$C_{20}H_{32}Fe_2K_2N_{16}O_4$
Formula weight	375.26	375.26	750.51
Crystal system	monoclinic	monoclinic	cubic
Space group	$P2_1/n$	$P2_1/n$	$Fm\bar{3}m$
$a/\text{\AA}$	9.13650(10)	11.8245(2)	11.9108(9)
$b/\text{\AA}$	11.7020(2)	11.7157(3)	11.9108(9)
$c/\text{\AA}$	15.6616(2)	11.9825(2)	11.9108(9)
$\alpha/^\circ$	90	90	90
$\beta/^\circ$	102.6670(10)	91.798(2)	90
$\gamma/^\circ$	90	90	90
Volume/ \AA^3	1633.71(4)	1659.15(6)	1689.8(4)
Z	4	4	2
Density/g \cdot cm $^{-3}$	1.526	1.502	1.475
R_1	0.0431	0.0532	0.0539
wR_2	0.1137	0.1539	0.1519
GOF	1.048	1.067	1.157

Table S4. Crystal data and structure refinement of EAOH-1 after heating to ITP at 100 K and 300 K.

Compound	EAOH-1	
Temperature	100 K	300 K
Formula	$C_{10}H_{16}FeKN_8O_2$	$C_{10}H_{16}FeKN_8O_2$
Formula weight	375.26	375.26
Crystal system	monoclinic	monoclinic
Space group	$P2_1/n$	$P2_1/n$
$a/\text{\AA}$	11.6613(4)	11.7784(5)
$b/\text{\AA}$	11.5994(4)	11.6709(4)
$c/\text{\AA}$	11.9561(4)	11.9663(5)
$\alpha/^\circ$	90	90
$\beta/^\circ$	92.675(3)	92.024(3)
$\gamma/^\circ$	90	90
Volume/ \AA^3	1615.47(10)	1643.93(12)
Z	4	4
Density/g·cm ⁻³	1.543	1.516
R_1	0.0379	0.0456
wR_2	0.0997	0.1116
GOF	1.096	1.082

Table S5. Selected geometric parameters (\AA , $^\circ$) for EAOH-1.

300 K (LTP)		368 K (ITP)		388 K (HTP)	
Bond Lengths	Experimental	Bond Lengths	Experimental	Bond Lengths	Experimental
Fe1—C1	1.942(4)	Fe1—C1	1.955(2)	Fe1—C1	
Fe1—C2	1.938(4)	Fe1—C2	1.942(2)	Fe1—C1 ¹	
Fe1—C3	1.942(3)	Fe1—C3	1.934(2)	Fe1—C1 ²	
Fe1—C4	1.940(4)	Fe1—C4	1.944(2)	Fe1—C1 ³	1.944(7)
Fe1—C5	1.944(3)	Fe1—C5	1.938(2)	Fe1—C1 ⁴	
Fe1—C6	1.944(3)	Fe1—C6	1.943(2)	Fe1—C1 ⁵	
K1—N1	2.827(3)	K1—N1 ¹	2.9685(19)	K1—N1 ⁶	
K1—N2 ⁴	2.862(3)	K1—N2 ²	2.854(2)	K1—N1 ⁷	
K1—N3 ¹	3.095(3)	K1—N3	2.8476(19)	K1—N1 ⁸	
K1—N4 ¹	3.214(4)	K1—N4 ³	2.916(2)	K1—N1 ⁹	2.886(6)
K1—N5 ²	2.861(3)	K1—N5 ⁴	2.853(2)	K1—N1 ¹⁰	
K1—N6 ³	2.869(3)	K1—N6 ⁵	2.906(2)	K1—N1 ¹¹	
K1—O1	2.951(3)				
N1—C1	1.146(5)	N1—C1	1.137(3)	N1—C1	
N2—C2	1.147(5)	N2—C2	1.143(3)	N1—C1 ¹⁴	
N3—C3	1.145(4)	N3—C3	1.145(3)	N1—C1 ¹⁷	
N4—C4	1.148(5)	N4—C4	1.137(3)	N1—C1 ¹⁸	1.186(9)
N5—C5	1.144(5)	N5—C5	1.148(3)		
N6—C6	1.151(5)	N6—C6	1.147(3)		
Bond Angles	Experimental	Bond Angles	Experimental	Bond Angles	Experimental
C1—Fe1—C2	89.24(16)	C1—Fe1—C2	92.65(9)	C1—Fe1—C1 ¹	
C1—Fe1—C3	90.49(15)	C1—Fe1—C3	89.66(9)	C1—Fe1—C1 ²	
C1—Fe1—C5	91.14(16)	C1—Fe1—C5	88.68(8)	C1—Fe1—C1 ³	
C1—Fe1—C6	91.69(14)	C1—Fe1—C6	89.99(8)	C1—Fe1—C1 ⁴	90.0
C2—Fe1—C3	90.47(14)	C2—Fe1—C3	89.25(10)	C1 ¹ —Fe1—C1 ³	
C2—Fe1—C5	89.13(14)	C2—Fe1—C5	88.09(9)	C1 ¹ —Fe1—C1 ⁵	
N1—K1—N2 ⁴	99.25(11)	N1 ² —K1—N2 ¹	88.40(6)	N1 ⁶ —K1—N1 ⁷	89.31(5)
N1—K1—N3 ¹	109.11(10)	N1 ² —K1—N4 ³	85.77(6)	N1 ⁶ —K1—N1 ¹⁰	102.6(4)
N1—K1—N4 ¹	82.54(9)	N1 ² —K1—N5 ⁵	90.94(5)	N1 ⁶ —K1—N1 ¹²	77.4(4)
N1—K1—N5 ²	108.88(10)	N1 ² —K1—N6 ⁴	92.43(5)	N1 ⁶ —K1—N1 ¹³	96.3(2)
N2 ⁴ —K1—N5 ²	88.69(10)	N2 ¹ —K1—N3	90.09(6)	N1 ⁸ —K1—N1 ⁹	96.3(2)
N2 ⁴ —K1—N6 ³	82.33(11)	N2 ¹ —K1—N5 ⁵	96.97(7)	N1 ⁸ —K1—N1 ¹⁰	89.31(5)
N1—C1—Fe1	177.9(4)	N1—C1—Fe1	178.8(2)	N1 ¹⁵ —C1—Fe1	
N2—C2—Fe1	178.0(3)	N2—C2—Fe1	177.8(2)	N1 ¹⁷ —C1—Fe1	164.5(5)
N3—C3—Fe1	176.9(3)	N3—C3—Fe1	177.8(2)	N1 ¹⁸ —C1—Fe1	
C1—N1—K1	156.2(3)	C1—N1—K1 ⁶	177.12(18)		
C2—N2—K1 ⁴	154.1(3)	C2—N2—K1 ⁷	167.2(2)	C1—N1—K1	158.1(7)
C3—N3—K1 ¹	93.0(2)	C3—N3—K1	176.28(16)		

Symmetry code(s) at 300 K: ¹1-X,1-Y,1-Z; ²1/2-X,-1/2+Y,3/2-Z; ³+X,-1+Y,+Z; ⁴-X,1-Y,1-Z; ⁵1/2-X,1/2+Y,3/2-Z;⁶+X,1+Y,+Z

Symmetry code(s) at 368 K: $^11/2+X, 1/2-Y, -1/2+Z; ^2+X, +Y, -1+Z; ^31/2-X, 1/2+Y, 1/2-Z; ^41/2-X, -1/2+Y, 1/2-Z; ^5-1/2+X, 1/2-Y, -1/2+Z; ^6+X, +Y, 1+Z; ^7-1/2+X, 1/2-Y, 1/2+Z; ^81/2+X, 1/2-Y, 1/2+Z$

Symmetry code(s) at 388 K: $^11-Y, 1/2-Z, 1/2-X; ^2+Y, 1/2+Z, -1/2+X; ^31/2+Z, +X, -1/2+Y; ^41/2-Z, 1-X, 1/2-Y; ^51-X, 1-Y, -Z; ^61/2-Z, -Y, -1/2+X; ^71/2-Z, 1/2-X, -Y; ^81-X, +Z, +Y; ^91/2-Y, 1/2-X, -Z; ^{10}1/2+Y, +Z, -1/2+X; ^{11}1-X, -Y, -Z; ^{12}1/2-Y, -Z, 1/2-X; ^{13}1/2+Y, -1/2+X, +Z; ^{14}1/2+Z, -1/2+X, +Y; ^{15}1/2+Z, +Y, 1/2-X; ^{16}+X, -Z, -Y; ^{17}1/2-Z, +Y, 1/2-X; ^{18}+X, +Y, -Z$

Table S6. Selected geometric parameters (\AA , $^\circ$) for EAOH-1 after heating to ITP.

100 K		300 K	
Bond Lengths	Experimental	Bond Lengths	Experimental
Fe1—C1	1.948(3)	Fe1—C1	1.948(3)
Fe1—C2	1.946(3)	Fe1—C2	1.947(3)
Fe1—C3	1.947(3)	Fe1—C3	1.944(4)
Fe1—C4	1.948(3)	Fe1—C4	1.943(3)
Fe1—C5	1.944(3)	Fe1—C5	1.943(3)
Fe1—C6	1.946(3)	Fe1—C6	1.943(4)
K2—N1 ¹	2.878(2)	K1—N1 ¹	2.903(3)
K2—N2 ²	2.822(3)	K1—N2 ²	2.959(3)
K2—N3	2.815(2)	K1—N3	2.836(3)
K2—N4 ³	2.944(3)	K1—N4 ³	2.838(3)
K2—N5 ⁴	2.818(2)	K1—N5 ⁴	2.845(3)
K2—N6 ⁵	2.881(2)	K1—N6 ⁵	2.907(3)
N1—C1	1.157(4)	N1—C1	1.140(5)
N2—C2	1.151(4)	N2—C2	1.146(4)
N3—C3	1.151(4)	N3—C3	1.140(5)
N4—C4	1.156(4)	N4—C4	1.138(4)
N5—C5	1.154(4)	N5—C5	1.146(5)
N6—C6	1.155(4)	N6—C6	1.144(5)
Bond Angles	Experimental	Bond Angles	Experimental
C1—Fe1—C2	90.00(11)	C1—Fe1—C2	89.98(13)
C1—Fe1—C4	89.60(11)	C1—Fe1—C4	89.92(14)
C1—Fe1—C5	90.29(11)	C1—Fe1—C5	89.87(15)
C1—Fe1—C6	91.76(11)	C1—Fe1—C6	91.28(15)
C2—Fe1—C3	91.50(11)	C2—Fe1—C3	88.64(14)
C2—Fe1—C5	88.49(11)	C2—Fe1—C5	92.68(14)
N1 ¹ —K2—N2 ⁴	92.83(7)	N1 ¹ —K1—N2 ²	91.76(9)
N1 ¹ —K2—N4 ²	89.20(7)	N1 ¹ —K1—N4 ⁴	90.05(10)
N1 ¹ —K2—N5 ⁵	102.34(7)	N1 ¹ —K1—N5 ⁵	102.93(12)
N1 ¹ —K2—N6 ³	84.34(7)	N1 ¹ —K1—N6 ³	82.31(11)
N2 ⁴ —K2—N3	86.89(7)	N2 ² —K1—N3	91.09(9)
N2 ⁴ —K2—N5 ⁵	89.54(7)	N2 ² —K1—N5 ⁵	87.80(9)
N1—C1—Fe1	177.9(3)	N1—C1—Fe1	178.1(4)
N2—C2—Fe1	178.5(2)	N2—C2—Fe1	177.2(3)
N3—C3—Fe1	176.5(3)	N3—C3—Fe1	176.4(4)
C1—N1—K2 ⁶	151.3(2)	C1—N1—K1 ⁶	154.6(3)

C2—N2—K2 ⁷	175.0(2)	C2—N2—K1 ⁷	175.7(3)
C3—N3—K2	162.3(2)	C3—N3—K1	167.7(3)
Symmetry code(s) at 100 K: ¹ +X,-1+Y,+Z; ² 3/2-X,-1/2+Y,3/2-Z; ³ 1-X,-Y,1-Z; ⁴ 3/2-X,-1/2+Y,1/2-Z; ⁵ 2-X,-Y,1-Z; ⁶ +X,1+Y,+Z; ⁷ 3/2-X,1/2+Y,1/2-Z; ⁸ 3/2-X,1/2+Y,3/2-Z			
Symmetry code(s) at 100 K: ¹ +X,1+Y,+Z; ² 1/2-X,1/2+Y,1/2-Z; ³ -X,1-Y,-Z; ⁴ 1/2-X,1/2+Y,-1/2-Z; ⁵ 1-X,1-Y,-Z; ⁶ +X,-1+Y,+Z; ⁷ 1/2-X,-1/2+Y,1/2-Z; ⁸ 1/2-X,-1/2+Y,-1/2-Z			

Table S7. The Elastic modulus (*E*) and Hardness (*H*) of selected HOIPs.

Compound	Elastic modulus (<i>E</i>) / GPa	Hardness (<i>H</i>) / GPa
[C ₄ H ₉ NH ₃] ₂ PbI ₄ ¹	3.3	-
[C ₆ H ₁₃ NH ₃] ₂ PbI ₄ ¹	2.1	-
(S)[C ₉ H ₁₁ NH ₃] ₂ PbI ₄ ¹	7.3	-
[C ₈ H ₉ NH ₃] ₂ PbI ₄ ¹	12.3	-
(S)[C ₉ H ₁₁ NH ₃][C ₃ H ₇ NH ₃]PbI ₄ ¹		
(S)[C ₉ H ₁₁ NH ₃][C ₄ H ₉ NH ₃]PbI ₄ ¹		
(S)[C ₉ H ₁₁ NH ₃][C ₆ H ₁₃ NH ₃]PbI ₄ ¹		7~9
(S)[C ₉ H ₁₁ NH ₃][C ₈ H ₁₇ NH ₃]PbI ₄ ¹		
(S)[C ₉ H ₁₁ NH ₃][C ₈ H ₉ NH ₃] ₂ PbI ₄ ¹		
[C ₇ H ₇ NH ₃] ₂ PbBr ₄ ²	16.9	-
CH ₃ NH ₃ PbI ₃ (100) face ³	14.3	0.57
CH ₃ NH ₃ PbI ₃ (112) face ³	14.0	0.55
CH ₃ NH ₃ PbBr ₃ (100) face ³	19.6	0.36
CH ₃ NH ₃ PbCl ₃ ⁴	26.119	-
CH ₃ NH ₃ SnI ₃ ⁴	23.271	-
CH ₃ NH ₃ SnBr ₃ ⁴	25.818	-
CH ₃ NH ₃ SnCl ₃ ⁴	30.836	-
CH ₃ NH ₃ PbBr ₃ (110) face ⁵	11.7	-
CH ₃ NH ₃ PbI _{3-x} Cl _x (h _c /t _f =9%) ⁶	19.65	0.78
(NH ₃ C ₈ H ₁₆ NH ₃)(CH ₃ NH ₃)Pb ₂ I ₇ ⁷	8.59	0.61
NH ₃ C ₄ H ₈ NH ₃ PbI ₄ ⁷	11.30	0.67
C ₆ H ₁₀ NH ₃ PbI ₄ ⁷	10.05	0.75
(C ₄ N ₂ H ₁₂)(NH ₄ Cl ₃)H ₂ O (111) face ⁸	24.02	-
(C ₄ N ₂ H ₁₂)(NH ₄ Cl ₃)H ₂ O (010) face ⁸	53.28	-
(C ₄ N ₂ H ₁₂)(NH ₄ Br ₃)H ₂ O (111) face ⁸	22.68	-
(C ₄ N ₂ H ₁₂)(NH ₄ Br ₃)H ₂ O (010) face ⁸	49.49	-
(C ₄ N ₂ H ₁₂)(NH ₄ I ₃)H ₂ O (111) face ⁸	18.82	-
(C ₄ N ₂ H ₁₂)(NH ₄ I ₃)H ₂ O (010) face ⁸	43.45	-
(C ₄ H ₁₁ CIN)CdCl ₃ (-205) face ⁹	52.21	-
(C ₄ H ₁₁ CIN)CdCl ₃ (100) face ⁹	31.65	-

Table S8. The elastic modulus (E) and hardness (H) of the three compounds (EA, EAOH-1 and EAOH-2) at room temperature and EAOH-1 in different phases.

Compound	E (GPa)	H (GPa)	Compound	E (GPa)	H (GPa)
EA, 295 K	8.82	0.26	EAOH-1, 295 K-1	36.68	0.98
EAOH-2, 295 K	21.09	0.38	EAOH-1, 363 K	13.99	0.17
EAOH-1, 295 K	36.68	0.98	EAOH-1, 296 K-2	15.34	0.30

References:

1. A. Negi, L. Yan, C. Yang, Y. Yu, D. Kim, S. Mukherjee, A. H. Comstock, S. Raza, Z. Wang, D. Sun, H. Ade, Q. Tu, W. You and J. Liu, *ACS Nano*, 2024, **18**, 14218-14230.
2. G. Feng, Y. Qin, C. Ran, L. Ji, L. Dong and W. Li, *APL Mater.*, 2018, **6**, 114201.
3. Y. Rakita, S. R. Cohen, N. K. Kedem, G. Hodges and D. Cahen, *MRS Commun.*, 2015, **5**, 623-629.
4. J.-H. Lee, Z. Deng, N. C. Bristowe, P. D. Bristowe and A. K. Cheetham, *J. Mater. Chem. C*, 2018, **6**, 12252-12259.
5. A. M. Lomonosov, X. Yan, C. Sheng, V. E. Gusev, C. Ni and Z. Shen, *Phys. Status Solidi-Rapid Res. Lett.*, 2016, **10**, 606-612.
6. A. A. Mamun, Y. Mohammed, T. T. Ava, G. Namkoong and A. A. Elmoustafa, *Mater. Lett.*, 2018, **229**, 167-170.
7. Q. Tu, I. Spanopoulos, E. S. Vasileiadou, X. Li, M. G. Kanatzidis, G. S. Shekhawat and V. P. Dravid, *ACS Appl. Mater. Interfaces*, 2020, **12**, 20440-20447.
8. K. Li, L.-Y. Dong, H.-X. Xu, Y. Qin, Z.-G. Li, M. Azeem, W. Li and X.-H. Bu, *Mater. Chem. Front.* 2019, **3**, 1678-1685.
9. T.-M. Guo, F.-F. Gao, Z.-G. Li, Y. Liu, M.-H. Yu and W. Li, *APL Mater.*, 2020, **8**, 101106.